CONF-850810--28

CONF-850810--28

DE85 018394

FREEZING CONTROLLED PENETRATION OF MOLTEN METALS FLOWING THROUGH STAINLESS STEEL TUBES

J. J. Sienicki, B. W. Spencer, D. L. Vetter, and R. H. Wesel
Reactor Analysis and Safety Division
Argonne National Laboratory
9700 South Cass Avenue
Argonne, Illinois 60439
(312) 972-4754

ABSTRACT

The freezing controlled penetration potential of molten metals flowing within stainless steel structure is important to the safety assessment of hypothetical severe accidents in liquid metal reactors. A series of scoping experiments has been performed in which molten stainless steel and nickel at various initial temperatures and driving pressures were injected downward and upward into 6.4 and 3.3 mm ID stainless steel tubes filled with argon gas and initially at room temperature. In all tests, there was no evidence that the solid tube wall was wetted by the molten metals. The penetration phenomena are markedly different for downward versus upward injections. The dependency upon tube orientation is explained in terms of the absence of wetting. Complete plugs were formed in all experiments halting the continued injection of melt. Calculations with a fluid dynamics/heat transfer computer code show that the injected masses limited by plugging are consistent with freezing through the growth of a stable solidified layer (crust) of metal upon the solid tube wall.

INTRODUCTION

The freezing controlled penetration potential of molten core fuel and structural materials flowing within stainless steel channels is important to the safety assessment of hypothetical severe accidents in liquid metal reactors (LMR's). The ability of disrupted core materials to penetrate through the flow channels defined by the fuel pins, subassembly hexcans, and various support structures plays an important role in determining the mode and timing of fuel escape from the disrupted core and the subsequent migration of fuel inside the reactor vessel. Previous experimental investigations of the freezing controlled penetration of molten reactor materials have concentrated upon the behavior of oxide fuel[1-6] or have employed simulant material tests[7-14] to study fundamental phenomena. Less common have been experiments[15] and analyses[16,17] investigating the freezing and plugging behavior of molten structural materials (i.e., molten ferrous alloys and alloying elements). In an oxide fueled LMR, the flow of molten structure (mainly stainless steel) may precede the dispersal of fuel through the escape paths leading from the disrupted core. Furthermore, current LMR concepts are examining the use of metal alloy fuel (predominantly metallic uranium alloyed with plutonium and/or zirconium) as an alternative to oxide fuel.

As discussed by Kondic,[18] the penetration phenomena for molten metals may differ significantly from those of ordinary liquids such as water because many metals do not wet the walls of the flow channel. Kolling and Grigull[19] presented a numerical model for predicting the penetration of flowing molten metals assuming that freezing occurs through the growth of a stable solidified layer, or crust, upon the channel wall. In their analysis, they assumed an imperfect thermal contact between the solid crust layer and the channel wall as modeled by a narrow air gap reflecting thermal contraction of the crust. Their model successfully predicted the results of experiments carried out with molten tin, lead, zinc, and aluminum.

A program of reactor material experiments has been initiated at ANL to investigate and characterize the interactions between flowing molten structure and flowing molten metal fuel with the stainless steel structure and sodium coolant under simulated hypothetical accident conditions. Presented here are the results and analysis of an initial series of scoping tests in which molten stainless steel and nickel were injected upward and downward into stainless steel circular tubes. The objectives are to determine the fundamental mechanisms underlying the freezing and penetration behavior of molten structure or metal fuel flowing through stainless steel channels and to predict the penetration achieved in the presence of freezing upon the channel wall.

DISCLAIMER

EXPERIMENT DESCRIPTION

Two molten metals were employed in the tests: stainless steel (Type 304) having solidus and liquidus temperatures of 1703 and 1738 K[20] and pure nickel with a melting/freezing temperature of 1728 K. The melts were injected into Type 304 stainless steel tubes filled with argon gas and initially at room temperature. The tube inner diameter was equal to 6.4 mm for the injections of stainless steel and 3.3 mm for the nickel injections. The molten melt superheat (i.e., excess temperature above the liquidus) was varied from values near zero to a maximum of approximately 200 K while the pressure drop driving the melts into the tubes ranged from as low as 0.0069 MPa (1 psig) for downward injection under near gravity drainage conditions to as much as 0.10 MPa for upward injection.

The electrically heated furnace used to melt and heat the injectant metals is shown in Figure 1 configured for the downward melt injection (DMI) experiments. The melt is held within a magnesia crucible and released by actuating the operating cylinder which raises a zirconia rod initially plugging a circular hole at the bottom of the crucible. Upon release, the melt drains out of the crucible through the cylindrical hearth region, melts through a thin diaphragm sealing the bottom of the furnace, flows into a second crucible resting inside a cooling spool/thermal standoff, and flows through a 1.27 cm diameter hole at the bottom of the second crucible leading to a conical entrance region to the tubular test section. The entire furnace may be pressurized with argon gas to a maximum pressure of ~ 0.2 MPa (15 psig) to create a pressure drop across the injected melt.

Figure 2 shows the apparatus configuration employed for the majority of the upward melt injection (UMI) experiments. The tubular test section is attached to a linear motion piston traveling within an air cylinder mounted atop a hollow cylinder inside which the tube moves down and up. The hollow cylinder is attached to the top of the furnace and is pressurized together with the furnace. When the melt has been heated to the desired temperature, the piston/cylinder assembly is actuated to lower the tube into the furnace to a preset depth beneath the surface of the melt. For the tests carried out with 6.4 and 3.3 mm ID tubes, the tube inlet was immersed to depths of 3.0 and 1.9 cm respectively. Following a preselected time interval (usually 3 s), the piston/cylinder assembly is again actuated to withdraw the tube from the furnace. In the upward melt injection tests, two procedures have been employed to produce a pressure gradient across the injected melt. In UMI-1 and -2, the tube was first inserted into the melt prior to pressurization of the furnace volume. When the tube was completely immersed, furnace pressurization was initiated providing a pressure drop which rises to a peak value over a timescale of ~ 0.14 s. For UMI-3 to -11, the furnace and tube were first pressurized to the desired level of overpressure before tube insertion. Upon full immersion, the tube was vented to the ambient pressure downstream of the tube exit employing the setup illustrated in Figure 2. This procedure results in a pressure drop which increases more rapidly to the desired level and remains essentially constant thereafter. For the UMI tests utilizing the smaller 3.3 mm ID tubes, the initial portion of the tube was machined to create a rounded entrance region 4.1 mm long over which the channel diameter decreases gradually from the 7.9 mm tube OD to the nominal 3.3 mm ID to minimize potential inlet flow head loss effects. Prior to each experiment the tube inner surface was cleaned successively with acetone, alcohol, and distilled water.

Test instrumentation consisted principally of a strain gauge type pressure transducer mounted atop the furnace to measure the furnace pressure and a Type R (Pt vs. Pt-13% Rh) thermocouple protected with a ceramic sheath which was immersed directly into the melt pool. For upward injections, the melt thermocouple was nominally positioned at the same depth as the tube inlet upon full insertion, while for injection in the downward direction, the thermocouple was located near the bottom of the pool. Additional heatup data was obtained from: (a) an optical pyrometer viewing the outer surface of the crucible through a circular quartz glass viewport in the furnace wall and a circular hole in the cylindrical heater element, and (b) a graphite thermocouple located opposite the viewport and at the same radius as the heater element. Throughout the heatup and injection phases, the melt temperature and furnace pressure were recorded with a strip chart recorder. During the injection phase, the furnace pressure as well as timing signals indicating the onset of tube lowering, full tube insertion, and the beginning of tube withdrawal were recorded using a Honeywell fibre-optic oscillographic recorder.

Following each experiment, the test section was radiographed to document the disposition of solidified metal within the tube. Subsequently, the short region of tube at the inlet which had been dipped into the melt and is embedded in a mass of solidified melt (upward injection) or penetrating slightly into the mounting flange (downward injection) was cut off and the mass of the melt within the short tube segment estimated. The predominant portion of the solidified injected metal inside the long tube segment downstream of the cut was physically removed and directly weighed thereby permitting a determination of the total injected mass.

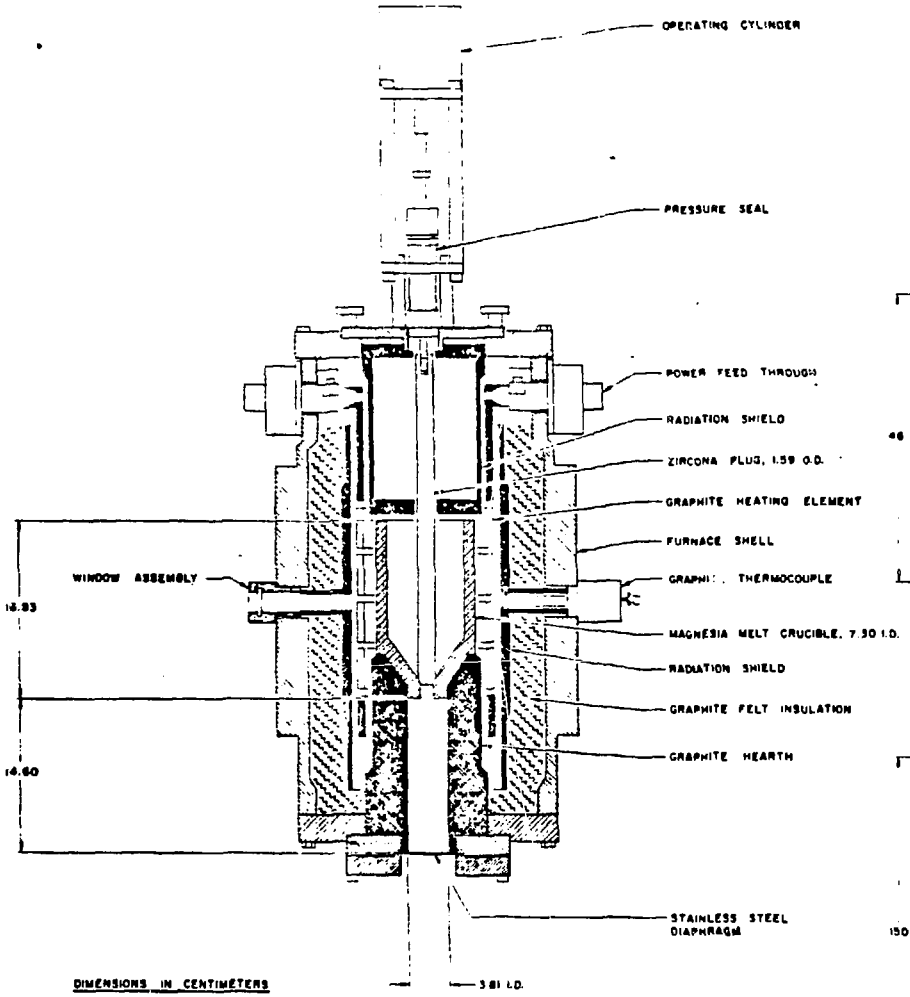

Fig. 1. Furnace Used to Melt Metals in Metal Freezing Experiments.

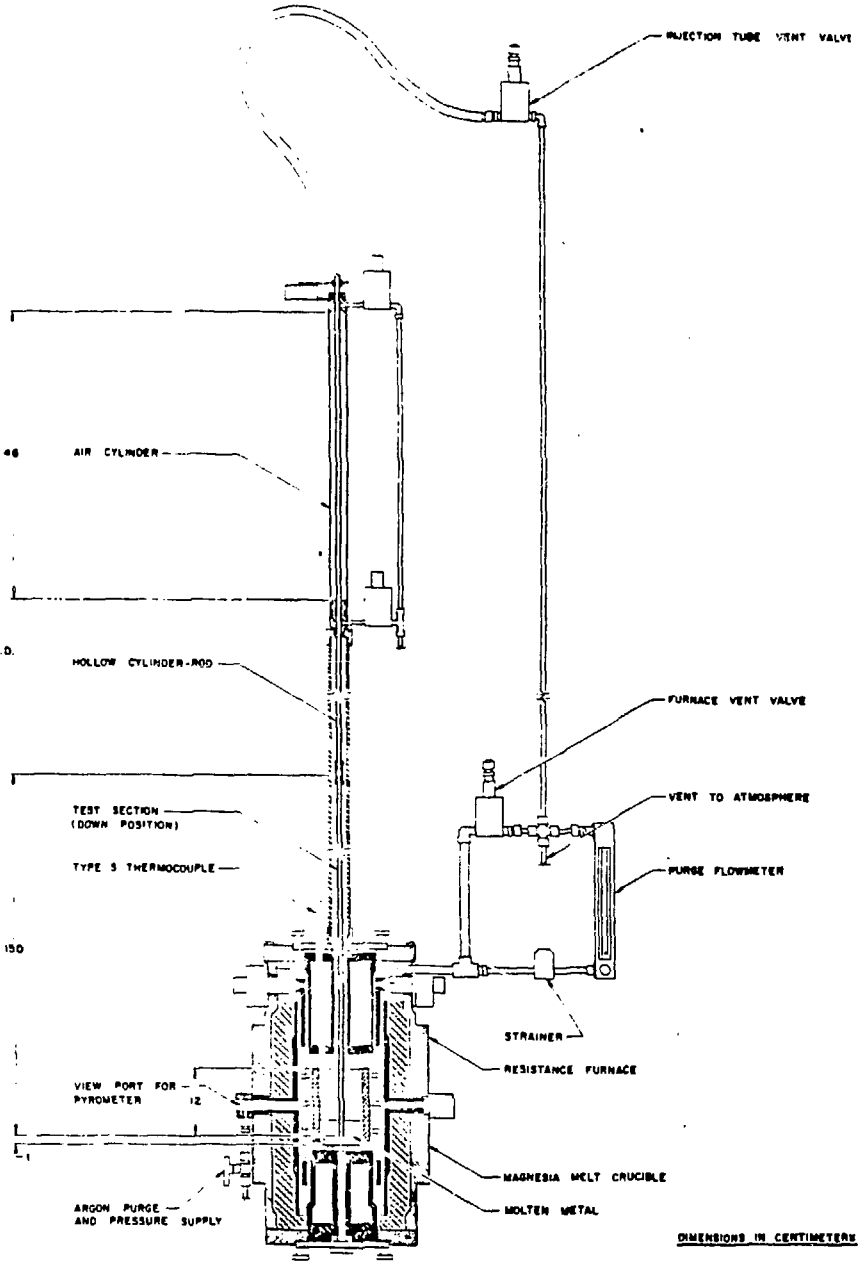

Fig. 2. Apparatus Employed for Upward Melt Injection Metal Freezing Experiments.

TABLE 1. CONDITIONS AND RESULTS OF METAL FREEZING EXPERIMENTS

Test	Melt	Tube ID/OD, mm	ΔP Maximum, MPa	Initial Melt Superheat, K	Crucible Metal Charge, kg	Tube Entrance Region	Maximum Melt Penetration, cm	Injected Mass,[1] g	Equivalent Penetration,[1,2] cm
DMI-4	SS	6.4/16	0.007	75	0.8	Conical[3]	95	110	45
UMI-1	SS	6.4/16	0.041	NA[4]	1.4	None	91	66	26
UMI-2	SS	6.4/16	0.029	9	1.4	None	9	23	9
UMI-3	SS	6.4/16	0.034	85[5]	1.0	None	44	100	41
UMI-4	SS	6.4/16	0.036	140	1.0	None	59	100	41
UMI-5	SS	6.4/16	0.070	160	1.0	None	72	170	68
UMI-7	Ni	3.3/7.9	0.035	200	1.0	Rounded[6]	28	12	16
UMI-8	Ni	3.3/7.9	0.035	43	1.0	Rounded	13	8	11
UMI-9[7]	Ni	3.3/7.9	0.035	27	1.0	Rounded	9	4	5
UMI-10	Ni	3.3/7.9	0.10	16	1.0	Rounded	48	8	11
UMI-11	Ni	3.3/7.9	0.069	16	1.0	Rounded	16	8	11

1. Downstream of entrance region
2. Based upon metal density at 298 K
3. Diameter decreases from 12.7 to 6.4 mm over a 6.4 mm length
4. Unknown due to early failure of melt thermocouple
5. Estimate based upon linear extrapolation of temperature following melt thermocouple failure
6. Diameter decreases from 7.9 to 3.3 mm over a 4.1 mm length
7. 0.79 mm diameter thermocouple inside channel along tube length; channel hydraulic diameter = 2.5 mm

EXPERIMENT RESULTS

Table 1 shows the conditions and results of the DMI/UMI experiments. Complete plugs were formed in all experiments, halting the continued injection of melt. A most interesting and significant result was that neither the molten stainless steel nor the molten nickel had wetted the solid stainless steel tube wall. The absence of wetting is evidenced by the convex shapes observed on the slugs of solidified metal which were easily removed from the tubes in posttest examination; the solidified metal was not "welded" to the tube wall. The surfaces of the solidified metal slugs were rough in texture containing numerous cavities and dents. While the extent of denting (e.g., the number of cavities per unit area) generally varies from test to test, the size of individual cavities appears to be related to the channel diameter with smaller dents obtained for the smaller diameter tubes. The occurrence of such surface cavities has been noted by previous investigators including Kolling and Grigull[19] for the freezing of flowing molten lead and is also implied by the drawings and results of Kuhn, Meechka, and Werle[15] for molten iron injected into quartz glass tubes. Because the initial temperature of the tube was not varied in the present test series, it is not known to what extent raising the initial stainless steel wall temperature might improve the wetting behavior.

One downward melt injection experiment, denoted DMI-4, was successfully performed in which molten stainless steel was injected downward under near gravity drainage conditions. Of the 110 g of melt which entered the tube, 71 g transcended the entire 95 cm tube length to form a molten pool inside a crucible placed beneath the tube exit. In posttest examination, 13 g of the injected steel was found to have formed a solid plug occluding the tube cross section up to 2.8 cm into the tube followed by a layer of melt covering a portion of the wall on one side of the tube and extending up to a distance of 11 cm downstream of the tube inlet. The remaining 30 g of melt removed from the tube comprised four slugs 5.5, 4.1, 4.2, and 3.5 cm in length with their leading edges located respectively at distances of 39, 43, 61, and 78 cm into the tube.

In contrast to the downward oriented experiment, in none of the upward directed tests did a significant mass penetrate the full 1 m tube length. In posttest examination of the upward melt injection experiments, the injected metal was seldom found in the form of a single solidified slug. Only for the UMI-2 test, in which the injected mass was relatively small, was a single slug observed. In UMI-3 and -5, the solidified metal ingots each consisted of two slugs separated by a short gap of void. For UMI-3, the upstream and downstream slug lengths were 9 and 34 cm respectively. The corresponding slug lengths measured in UMI-5 were 42 and 30 cm. For the remaining experiments, the solidified melts generally consisted of a relatively long slug encompassing the tube inlet and plugging the channel followed by a shorter "downstream region" comprised of a number of slugs. Individual slugs were usually separated by void or held together by layers or films of frozen melt adjacent to the tube wall. Such individual layers often formed only on one side of the tube wall covering a portion of the full channel circumference. The underlying mechanism responsible for the observed dispositions of solidified metal is unclear at the present time. The material dispositions are suggestive of an "inertial effect" in which the formation of a solid plug occluding the channel cross section brings the liquid upstream of the plug to an abrupt halt while the liquid downstream of the plug location continues its motion through the tube possibly breaking up into slugs or droplets. (It is also possible that some breakup might occur prior to the complete occlusion of the channel.) Alternatively, it is possible that the multidimensional flow pattern which develops near the tube inlet might result in the formation of a crater or depression in the free surface of the melt pool surrounding the tube such that the surface sometimes falls below the tube entrance permitting gas to enter the tube together with melt. In either case, the principle quantity of interest is the total mass injected into the tube. Using the total injected mass, an equivalent penetration based upon the assumption of a single continuous slug may be defined (Table 1). To partially indicate the extent of the "inertial effect" or "two-phase effect," Table 1 also shows the maximum penetration attained by any of the injected melt. It should be noted that the actual mass which achieves the maximum penetration may be quite small as in UMI-1 where only a single particle was found to have traveled the entire 91 cm tube length.

ANALYSIS OF DIFFERENCES BETWEEN DOWNWARD AND UPWARD INJECTION

The observed nonwetting of the solid stainless steel tube wall by the injected molten metals results in the prediction of qualitatively different penetration phenomena for injections carried out in the downward versus upward directions. For downward injection, the draining liquid stream will, in the absence of wetting, contract away from the wall as a result of its continuing acceleration under gravity. Kondic[18] has discussed this contraction phenomenon and its consequences in founding practice noting that downward channels of uniform cross section which run full with water will not do so with liquid metals due to the differences in the wetting characteristics of the two types of liquids. Kondic also notes that it is essential to use tapered channels (sprues) for metal flow, if an efficient downward flow in which the melt continues to fill the cross section is desired. In the absence of wetting, it is therefore expected that after entering the tube, the melt forms an inverted annular flow regime. Analagous to an unconfined liquid jet, the molten stream within the tube will break up as illustrated in Figure 3. Depending upon the flow conditions, breakup results in the formation of either liquid slugs or droplets. For DMI-4, the liquid stream beyond a distance of 22 cm into the tube is predicted[21] to break up into liquid slugs. Individual slugs can fall through the full length of the tube (95 cm) without undergoing significant heat loss (estimated $\lesssim$ 10 K on the basis of thermal radiation from the slugs to the wall). In the experiment, the greater portion (71 g) of the injected mass (110 g) was, in fact, retrieved as a solidified pool from the crucible placed beneath the tube exit.

In contrast, when melt is injected upward, gravity acts to decelerate the liquid stream causing it to fill the channel (Figure 3) such that conduction heat transfer to the wall and solidification can take place. The molten metal is thus expected to flow upward as a single liquid slug filling the available cross-sectional flow area.

PREDICTION OF INJECTED MASS AND PLUGGING

Analysis of the injected mass (or equivalent penetration) and plug formation was carried out using the EMP-C (Experiment Modeling Freezing-Conduction) coupled fluid dynamics/heat transfer computer code which calculates the conduction freezing controlled penetration of a melt within a freezing channel. Freezing is assumed to take place with the growth of a stable solidified layer, or crust, upon the channel wall (i.e., the stable crust growth/conduction model;[1] plugging occurs when the crust at some location grows to completely occlude the channel. For the metal freezing experiments, the code models the injected melt as a one-dimensional, growing length of incompressible liquid flowing through a circular channel possessing dimensions which vary in space and time to reflect the growth and remelt-

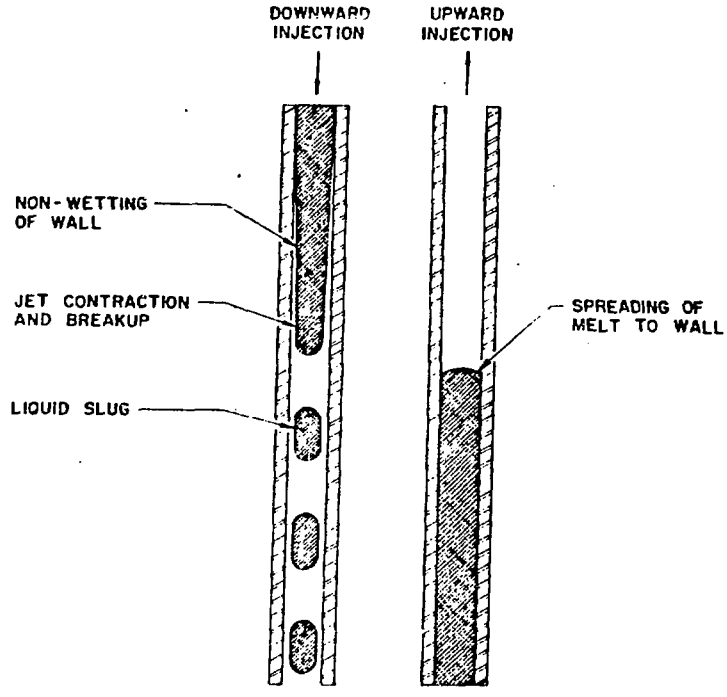

Fig. 3. Differences Between Downward and Upward Melt Injection.

ing of crust. Crust formation and conduction heat transfer within the crust and tube wall are calculated normal to the flow and assuming radial symmetry. To facilitate the calculation of the simultaneous growth of crust and heating of the tube wall, a fixed r-z mesh is defined upon the initial channel and tube wall. At each axial elevation, crust evolution is described by either of two methodologies depending upon the instantaneous crust thickness. The one-dimensional calculation of the dynamics of "thin" crusts having a thickness less than that of the outermost channel mesh cell employs the refined integral heat balance method of Volkov and Li Orlov[22] to account for the effects of the thermal profile within the crust. Thicker crusts are described with a radial finite difference calculation coupled to a continuous tracking of the melt/crust interface as it moves across the radial mesh cells at each axial level. The calculation of the heatup of the surrounding tube wall employs the refined integral heat balance approach until the thermal boundary layer reaches the center of the innermost wall mesh cell and then switches to a radial finite difference calculation. For the portion of the tube immersed in the pool, the code also calculates the freezing of melt upon the tube outer surface which enhances the heatup of the channel wall. For the remainder of the tube, a thermal radiation boundary condition is assumed at the wall outer surface. The calculation of fluid hydraulics (i.e., the momentum equation) interior to the crust in response to the applied pressure drop includes the effects of fluid inertia, turbulent and laminar friction, gravity, and entrance head loss effects at the tube inlet. The fluid mass and enthalpy equations are solved with a one-dimensional Lagrangian scheme in which the volume of each individual melt cell decreases or increases as melt is frozen out as crust or crust is remelted. The melt and wall materials are described with temperature dependent thermophysical properties. Calculations are continued until the crust at some axial level grows to completely occlude the channel.

In the present application, the heat transfer coefficient describing forced convection heat transfer from the flowing melt to the crust is taken equal to the maximum of two terms. The first is the correlation of Seban and Shimazaki,[23]

$$h = \left[5 + 0.025\ (RePr)^{0.8}\right] \frac{k}{D}, \qquad (1)$$

appropriate for liquid metal heat transfer with fully developed flow and a constant wall temperature. The second term is the transient conduction expression,

$$h = \frac{k}{\sqrt{\pi\alpha(t-t_e)}}, \qquad (2)$$

where t_e is the time at which the particular Lagrangian melt cell enters the channel.

A major assumption of the present analysis is that even though the melt does not actually wet the tube wall, the thermal contact between the crust and the wall may still be treated as perfect and ideal from a heat transfer standpoint (i.e., a significant effective thermal resistance does not develop at the crust/wall interface). This assumption is borne out by the comparison of model predictions with the experiment results. It is noteworthy that this approach is in contrast to that of Kolling and Grigull[19] who assumed that a narrow gap representing thermal contraction of the crust develops interstitial to the crust and tube wall thereby providing a heat transfer resistance. On the other hand, Kolling and Grigull did not include the contribution to forced convection heat transfer resulting from turbulent eddy transport across the width of the channel which is embodied in a correlation such as Equation 1. Ignoring the enhancement to heat transfer due to eddy convection might tend to offset the effects of a gap resistance.

The code was first applied to the downward melt injection experiment, DMI-4. Since the melt stream contracts after entering the tube, it was assumed that the molten steel contacts the wall and is solidified as a crust only in the vicinity of the tube inlet. Based upon posttest examination, crust formation is assumed to take place only over the first 2.8 cm of tube length (Figure 4). The freezing channel modeled in the calculation thus consists of the 6.4 mm long, conical entrance region inside the mounting flange within which the initial channel diameter decreases from 12.7 to 6.4 mm followed by a tube only 2.8 cm long. Beyond this distance, the liquid stream is envisioned to contract away from the wall and may be modeled with an outflow boundary condition. The calculation predicts that a complete plug forms at 0.72 s following the onset of injection occluding the channel at the downstream end of the crust region at 2.8 cm into the tube. At this time, the mass injected into the tube downstream of the flange/entrance region is calculated to equal 74 g compared with the measured mass of 110 g. The predicted injected mass is only 35% lower than the measurement such that the agreement between calculation and experiment is judged to be supportive of the stable crust/conduction freezing concept.

For the upward melt injection experiments, the molten metal fills the cross-sectional flow area. The code calculations were therefore carried out assuming that the melt contacts the tube wall and is solidified as a stable crust at all locations behind the melt leading edge (Figure 5). It is necessary to model the time dependant immersion of the tube into the molten pool. The gas volume downstream of the tube entrance is sufficiently large that molten metal can more or less freely enter the tube as it is lowered into the pool. Accordingly, the flow of melt into the tube during immersion is modeled with a constant velocity, inlet flow boundary condition equal to the insertion velocity over a time interval representative of downward tube motion through the pool (1.2 m/s over 0.026 s for UMI-1 to -5 and 0.95 m/s over 0.020 s for UMI-7 to -11).

The results of the code calculations are shown in Table 2. Analysis of UMI-1 was not undertaken, because the molten steel temperature at the time of injection is unknown due to the early failure of the thermocouple immersed in the melt pool. For UMI-2, the peak furnace pressure is known, but the actual pressure time history was not successfully recorded thereby precluding a calculation of UMI-2 as well.

For UMI-3 to -11, venting of the gas overpressure downstream of the tube was employed to create a rapid rise to an essentially constant driving pressure drop across the injected melt. The code calculations thus assume that immediately following the complete immersion of the tube, the pressure drop increases suddenly in a steplike fashion to the values in Table 2 and remains constant thereafter. The predicted injected masses downstream of the tube entrance region are in very good agreement with those obtained in the experiments. Specifically, the ratio of the calculated and experimental masses (or equivalent penetrations) has a lowest value of 0.84 (for UMI-9), a highest value of 1.20 (for UMI-4), and an average of 1.02 for the eight tests considered here. The degree of agreement obtained is strongly supportive of the stable crust growth freezing concept. For all of the Ni injections, plug formation (i.e., complete channel occlusion by the crust) is calculated to first occur immediately beyond the entrance region where the initial channel diameter first equals the nominal 3.3 mm tube ID. In contrast, for those tests involving the injection of molten stainless steel into 6.4 mm ID tubes, plugging takes place downstream of the inlet but still at a distance which is no greater than 46% of the leading edge penetration. In all calculations, complete plug formation is predicted before the melt leading edge has risen to a height such that the gravity head of the injected melt above the pool balances the applied maximum pressure drop.

Both the measured and predicted injected masses for UMI-9 are significantly less than those of comparable tests (e.g., UMI-8). In UMI-9, a 0.79 mm diameter thermocouple was located inside the tube along the channel length in an attempt to directly measure the temperature of the molten Ni entering the tube. The code calculation shows that the relatively small

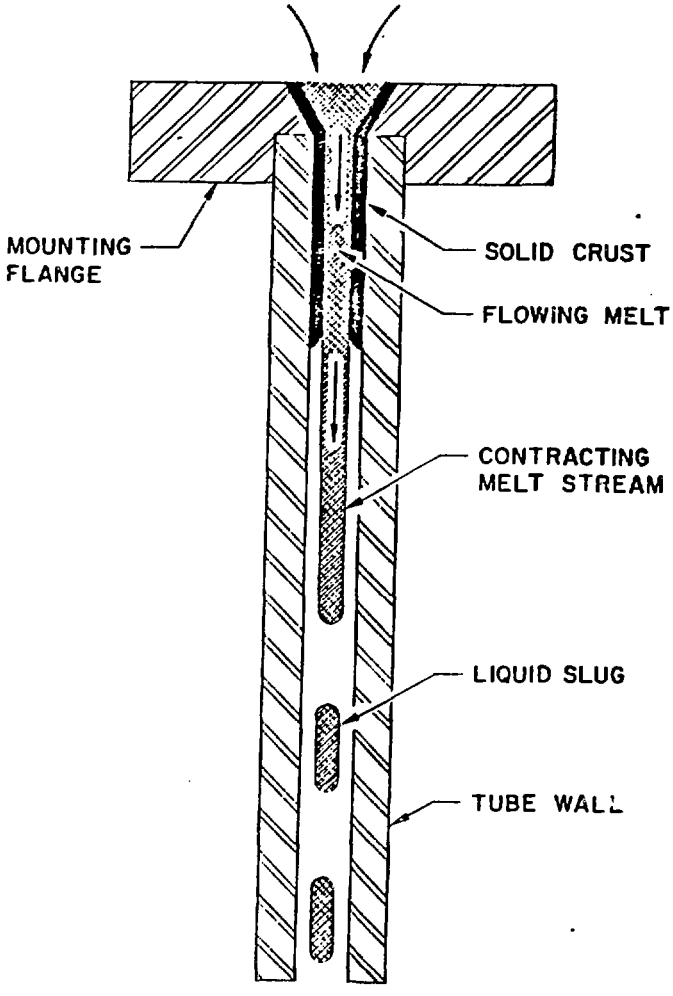

Fig. 4. Configuration Assumed for Calculation of Downward Melt Injection Experiment.

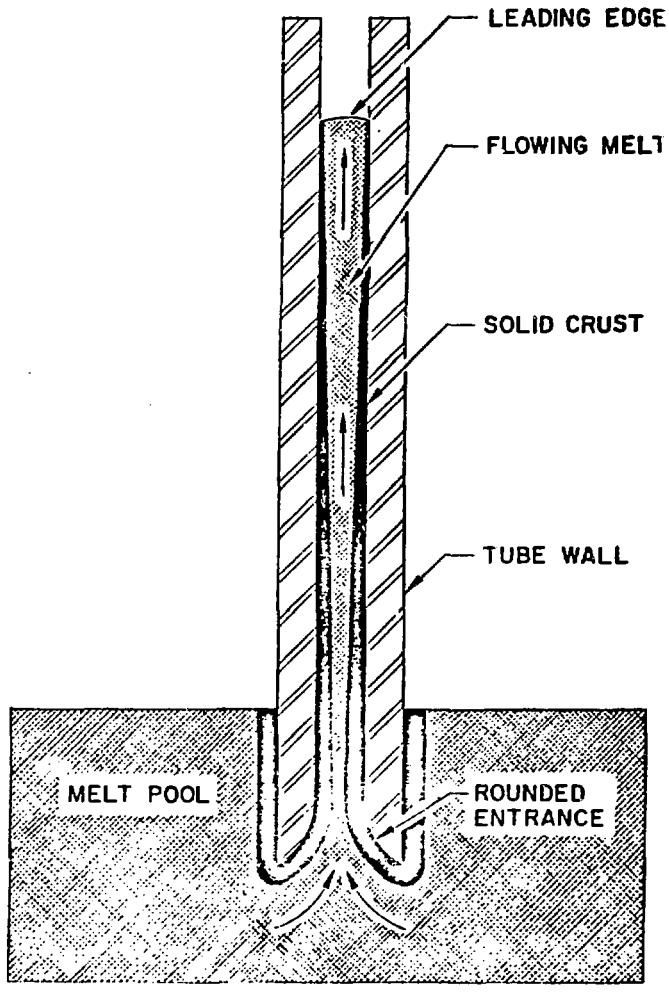

Fig. 5. Configuration Assumed for Calculation of Upward Melt Injection Experiments (Rounded Entrance Case Shown).

injected mass obtained in UMI-9 is caused by the reduction in the channel hydraulic diameter accompanying the inclusion of the thermocouple.

CONCLUSIONS

The following conclusions are drawn from the results of the metal freezing experiments and analysis:

i) For the injection of molten stainless steel and nickel into stainless steel circular tubes filled with argon and initially at room temperature, there is no evidence that the molten metals wet the solid tube wall as revealed by the convex shapes observed on solidified metal slugs which were easily removed from the tubes as well as the appearance of cavities or dents on the slug outer surfaces. Additional work is required to characterize the dependency of wetting behavior upon the initial wall temperature.

ii) There is a significant difference in behavior between injections carried out in the downward versus upward directions which may be explained in terms of the nonwetting of the tube wall by the melt. For downward injection in the absence of wetting, the melt stream contracts away from the wall due to gravitational acceleration breaking up into slugs or droplets which can fall through the entire tube length without undergoing significant additional heat loss. In contrast, for upward injection, the melt is decelerated by gravity and fills the cross-sectional flow area such that conduction heat transfer can take place at the wall resulting in stable crust formation upon the wall.

TABLE 2. PREDICTION OF METAL FREEZING EXPERIMENTS ASSUMING STABLE CRUST FORMATION AND PERFECT THERMAL CONTACT BETWEEN CRUST AND TUBE WALL

Test	Melt	Tube ID/OD, mm	ΔP Maximum, MPa	Initial Melt Superheat, K	Plugging Time, s	Plug Location, cm	Injected Mass,[1] g	Equivalent Penetration,[1] cm
DMI-4	SS	6.4/16	0.007	75	0.72	2.8	74	29
UMI-3	SS	6.4/16	0.034	85	0.71	15	110	45
UMI-4	SS	6.4/16	0.036	140	0.75	21	120	49
UMI-5	SS	6.4/16	0.070	160	0.75	32	170	69
UMI-7	Ni	3.3/7.9	0.035	200	0.16	0.0	11	14
UMI-8	Ni	3.3/7.9	0.035	43	0.13	0.0	7	10
UMI-9	Ni	2.5/7.9	0.035	27	0.070	0.0	3	4
UMI-10	Ni	3.3/7.9	0.10	16	0.12	0.0	10	13
UMI-11	Ni	3.3/7.9	0.069	16	0.12	0.0	8	11

1. Downstream of entrance region.

iii) In all experiments, complete plugs were formed halting the continued injection of melt. The masses injected into the tubes limited by plug formation are in good agreement with code calculations assuming the growth of a stable crust of solidified metal upon the solid tube wall, perfect thermal contact between the crust and the wall, and plugging when the crust completely occludes the channel. This is the case even for the downward oriented test in which crust formation was limited to only a short length at the tube inlet.

iv) The dispositions of solidified metal observed in posttest examination of the UMI tests might be the result of an inertial effect in which the molten metal downstream of the location of initial plug formation continues its motion through the channel following complete channel occlusion possibly breaking up into slugs or droplets.

ACKNOWLEDGEMENTS

This work was performed under the auspices of the U. S. Department of Energy. Figures were drawn by J. Logan. The manuscript was prepared by V. Eustace and M. Mehaffey.

NOTATION

D = hydraulic diameter, m

h = heat transfer coefficient, $W/(m^2 \cdot K)$

k = thermal conductivity, $W/(m \cdot K)$

Pr = Prandtl number

Re = Reynolds number

t = time, s

α = melt thermal diffusivity, m^2/s

ΔP = pressure drop across injected melt, Pa

LITERATURE CITED

1. M. Epstein, M. A. Grolmes, R. E. Henry, and H. K. Fauske, Nucl. Sci. Eng., 61, p. 310 (1976).

2. M. Epstein, R. E. Henry, M. A. Grolmes, H. K. Fauske, G. T. Goldfuss, D. J. Quinn, and R. L. Roth, "Analytical and Experimental Studies of Transient Fuel Freezing," Proceedings of the International Meeting on Fast Reactor Safety and Related Physics, Chicago, IL, October 5-8, 1976, CONF-761001, Vol. IV, p. 1788, United States Energy Research and Development Administration (1976).

3. B. W. Spencer, R. E. Henry, H. K. Fauske, G. T. Goldfuss, and R. L. Roth, "Summary and Evaluation of Reactor-Material Fuel Freezing Tests," Proceedings of the International Meeting on Fast Reactor Safety Technology, Seattle, WA, August 19-23, 1979, Vol. 4, p. 1766, American Nuclear Society (1979).

4. G. Maurin and M. Amblard, "An Approach of Molten Fuel Relocation Problem," Proceedings of the ENS/ANS International Topical Meeting on Nuclear Power Reactor Safety, Brussels, Belgium, October 16-19, 1978, Vol. 2, p. 1096, European Nuclear Society (1978).

5. D. A. McArthur, N. K. Hayden, and P. K. Mast, "In-Core Fuel Freezing and Plugging Experiments: Preliminary Results of the Sandia TRAN Series 1 Experiments," NUREG/CR-3675, SAND81-1726, Sandia National Laboratories (August 1984).

6. D. A. McArthur and P. K. Mast, "TRAN B-1: Experimental Investigation of Fuel Crust Stability on Surfaces of an Annular Flow Channel," NUREG/CR-3484, SAND83-1916, Sandia National Laboratories (January 1984).

7. F. B. Cheung and L. Baker, Jr., Nucl. Sci. Eng., 60, p. 1 (1976).

8. M. Epstein, A. Yim, and F. B. Cheung, Journal of Heat Transfer, 99, p. 233 (1977).

9. H. M. Chun, J. J. Barry, M. S. Kazimi, T. Ginsberg, and O. C. Jones, Jr., "Solidification Dynamics of Flowing Fluids," BNL-NUREG-24616, Brookhaven National Laboratory (1977).

10. A. Yim, M. Epstein, S. G. Bankoff, G. A. Lambert, and G. M. Hauser, Int. J. Heat Mass Transfer, 21, p. 1185 (1978).

11. G. A. Greene, O. C. Jones, Jr., M. S. Kazimi, J. J. Barry, and G. A. Zimmer, "Two-Phase Transient Solidification Dynamics of Flowing Fluids with Non-Condensable Vapors," BNL-NUREG-24486R (1978).

12. A. Ganguli and S. G. Bankoff, "Crust Behavior in Simultaneous Melting and Freezing on a Submerged Flat Plate," Heat Transfer-San Diego 1979, ed. R. W. Lyckowski, AIChE Symposium Series, No. 189, Vol. 75, p. 40, American Institute of Chemical Engineers, New York (1979).

13. M. Epstein, L. J. Stachyra, and G. A. Lambert, Journal of Heat Transfer, 102, p. 330 (1980).

14. S. W. Eisenhawer, D. O. Lee, M. L. Corradini, and R. W. Ostensen, "On the Physics of Fuel Streaming and Freezing in Fast Reactor Core Disruptive Accidents," NUREG/CR-2028, SAND80-0484, Sandia National Laboratories (August 1981).

15. D. Kuhn, M. Möschke, and H. Werle, "Freezing of Aluminum Oxide and Iron Flowing Upward in Circular Quartz Glass Tubes," KFK 3592, Kernforschungszentrum Karlsruhe (October 1983).

16. J. Szekely and S. T. DiNovo, Metallurgical Trans., 5, p. 747 (1974).

17. J. J. Sienicki and B. W. Spencer, Trans. Am. Nucl. Soc., 46, p. 508 (1984).

18. V. Kondic, Metallurgical Principles of Founding, p. 219-228, Edward Arnold Ltd., London (1968).

19. M. Kölling and U. Grigull, Wärme-und Stoffubertragung (Berlin), 14, p. 231 (1980).

20. Metals Handbook 1948 Edition, ed. T. Lyman, p. 399, American Society for Metals, Cleveland (1948).

21. G. De Jarlais, M. Ishii, and J. Linehan, "Hydrodynamic Stability of Inverted Annular Flow in an Adiabatic Simulation," Interfacial Transport Phenomena, ed. J. C. Chen and S. G. Bankoff, The American Society of Mechanical Engineers, New York (1983).

22. V. N. Volkov and V. K. Li-Orlov, Heat Transfer-Soviet Research, 2, p. 41 (1970).

23. R. A. Seban and T. T. Shimazaki, Trans. ASME, 73, p. 803 (1951).